IET Optoelectronics

Research Article

IET Journals
The Institution of Engineering and Technology

InAs/GaAs quantum dot solar cells with quantum dots in the base region

ISSN 1751-8768
Received on 1st July 2018
Revised 3rd January 2019
Accepted on 13th February 2019
E-First on 18th March 2019
doi: 10.1049/iet-opt.2018.5069
www.ietdl.org

Shun Chan[1], Dongyoung Kim[1] ✉, Ana M. Sanchez[2], Yunyan Zhang[1], Mingchu Tang[1], Jiang Wu[1], Huiyun Liu[1]

[1]*Department of Electronic and Electrical Engineering, University College London, Torrington Place, London, WC1E 7JE, UK*
[2]*Department of Physics, University of Warwick, Coventry CV4 7AL, UK*
✉ *E-mail: d.kim@ucl.ac.uk*

Abstract: In this work, the influence of quantum dot (QD) position on the performance of solar cells was studied. The presence of QDs within the base regions leads to improved open circuit voltage (V_{oc}) from 0.73 to 0.90 V. Despite a slight reduction in short-circuit current (J_{sc}) due to carrier collection loss, the enhancement of the V_{oc} of QDSCs with QDs in base region is significant enough to ensure that power conversion efficiencies (η) are higher than the reference quantum dot solar cell (QDSC) of which QDs are embedded in the intrinsic region. Moreover, sample with QDs in deep base region achieved the highest η of 9.75%, an increase of 29% with regard to the reference quantum dot solar cell.

1 Introduction

Over the past decades, great efforts have been devoted to realising solar cells (SCs) that can exceed the Shockley–Queisser limit of 31% [1]. Hot carrier SCs, multi-junction SCs and quantum dot solar cells (QDSCs) aim to improve the efficiency by utilising the solar spectrum more effectively [2, 3]. Amongst these, QDSCs have the potential to achieve intermediate band solar cells with a theoretical conversion efficiency up to 63.2% [4]. By introducing one additional energy level between conduction band (CB) and valence band (VB), photons with insufficient energy to pump electrons from VB to CB can use this intermediate band (IB) as a stepping stone to generate an electron-hole pair [5]. Quantum dots (QDs) have been employed in the practical implementation of such a concept. Due to their three-dimensional carrier confinement and discrete density of states, the energy levels of the confined states in a QD can be used as an IB [5–7]. However, there are several challenges that must be addressed before utilising high efficient QD solar cells.

Due to the small absorption volume of the QDs, their contribution to the total photocurrent is quite insignificant. To increase the QD absorption, the most obvious and effective approach is to grow multiple stacks of QDs. However, the self-assembled Stranski–Krastanov (S-K) growth usually results in the degradation of QD structure and generation of misfit dislocations [8]. To this extend, strain compensation layers (SCL) need to be deployed in order to accomplish ultra-high stacks of QDs. Reports have shown 40 stacks of QDs can be obtained by utilising GaP as a SCL [9]. We have also showed that photocurrent can be improved by increasing in-plane QD density. Another serious issue is the significant reduction in open circuit voltage (V_{oc}), which always counteracts the benefit of short-circuit current density increase (J_{sc}). The primary causes include the shrinkage of effective bandgap, radiative recombination via QDs, and non-radiative recombination caused by defects related to strain relaxation [10]. As a result, a number of efforts have been devoted to preventing the substantial voltage decrease in QDSCs. For example, intentional doping in QDs have been used to passivate the defect states or to form charge dots to suppress recombination [11]. Moreover, intentional n-type doping in QD, which exhibit negatively charged dots, can enhance the short-circuit current significantly without the deterioration of voltage [12].

From previous studies, QDs have either varied their position solely within the intrinsic region or have been inserted into different regions within an Multi-junction solar cell (MJSC) [13, 14]. The results were intriguing and hence provided us very insightful design structures. In this paper, we differ by studying the influence of QD positions within the base regions. Our primary aim is to recover voltage through the background n type doing. Indeed, open circuit voltage data have shown substantial increases by at least 20%.

2 Experimental details

QDSC samples were grown by a solid-source molecular beam epitaxy on GaAs (100) substrates. Fig. 1 illustrates the sample structures of (a) QDs in the shallow base region (shallow QD) and (b) QDs in the deep base region (deep QD), which can be confirmed by the TEM images (c) and (d), respectively. Both samples had a p-i-n structure consisting of a 200 nm n^+ GaAs buffer layer with Si doping level of 1×10^{18} cm^{-3}, a 30 nm n^+ $Al_{0.35}Ga_{0.65}As$ Back Surface Field with Si doping level of 1×10^{18} cm^{-3}, a 1000 nm n GaAs base region with Si doping level of 1×10^{17} cm^{-3}, a 420 nm i GaAs intrinsic region, a 250 nm p^- GaAs emitter region with Be doping level of 2×10^{18} cm^{-3}, a 30 nm p $Al_{0.8}Ga_{0.2}As$ window with Be doping level of 2×10^{18} m^{-3} and 50 nm p^+ GaAs contact layer with Be doping level of 1×10^{19} cm^{-3}. 20 layers of 2.1 monolayer (ML) InAs QDs separated by 20 nm GaAs spacer layer with Si doping level of 1×10^{17} cm^{-3} were grown into the top and the bottom section of the base region, indicated as shallow and deep respectively. The QDs were grown by the Stranski–Krastanov mode at a substrate temperature of ~500°C. High growth temperature GaAs spacer layers were applied during the growth of QDs to suppress the formation of dislocations [15, 16].

Post MBE-growth, samples were cleaved into quarter-wafers and cleaned using acetone and isopropanol for 10 min each. Surface oxides were removed by dipping the samples into diluted ammonia solution (1:19) for 50 s. 10 nm Ni/100 nm AuGe/30 nm Ni/200 nm Au were thermal evaporated onto the backside of the samples to form n-type contact. To enhance the formation of n-type ohmic contact, samples were thermally annealed at 420°C for 30 s following the thermal evaporation. For p-type ohmic contact, photolithography was performed to define the grid patterns

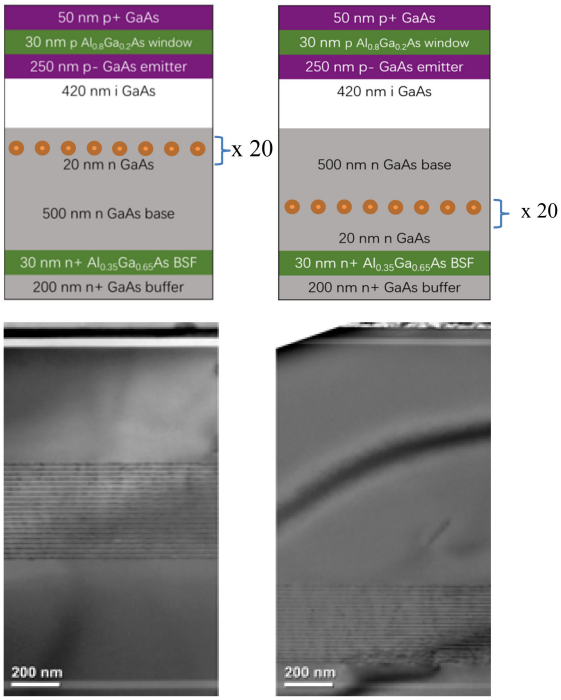

Fig. 1 *QDSC sample structures*

(a) QDs in shallow base region, ***(b)*** QDs in deep base region, ***(c)*** and ***(d)*** TEM images of QDs in base region

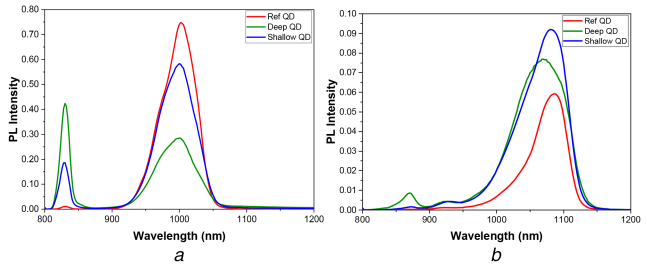

Fig. 2 *PL spectra of reference, deep region and shallow region QDSCs at* ***(a)*** 10 K, and ***(b)*** 300 K

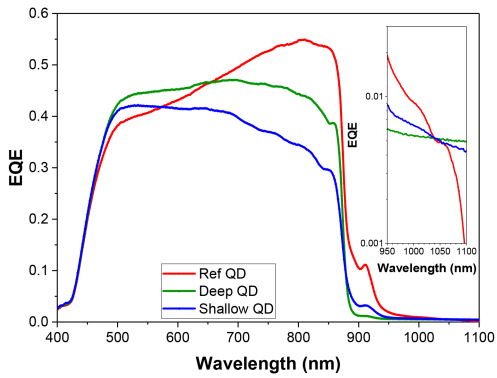

Fig. 3 *External quantum efficiency spectra with inset shows the sub-bandgap EQE in log-scale*

followed by the deposition of 20 nm Ti/50 nm Pt/400 nm Au via sputtering. Individual SC devices were isolated through wet etching which immersed the samples in an H_2SO_4:H_2O_2:H_2O (1:10:80) selective etching solution for 5 min. No anti-reflection coating was deposited during fabrication process.

Temperature dependent and power dependent PL spectra were obtained using 532 nm excitation from a diode pump solid-state laser and a helium cooled cryostat. Current density versus voltage (*J*–*V*) characteristics were measured by using a LOT calibrated solar simulator with a xenon lamp under one sun (AM1.5G) illumination at room temperature (RT). Photocurrent measurements were performed with the light beam of a halogen lamp chopped to a frequency of 188 Hz through a Newport monochromator. The monochromatic beam was calibrated with a GaAs photodiode and the data were analysed with Tracer 3.2 software to produce the External quantum efficiency (EQE).

3 Results and discussion

The optical properties of shallow QD and deep QD samples were compared with a reference QDSC (ref QD) where QDs are embedded in the intrinsic region. Fig. 2*a* shows the PL spectrum of the QDSCs at 10 K, two peaks positioned at 830 and 1000 nm correspond to the wavelengths of GaAs and InAs QDs. Narrow linewidth indicates that the material is in decent quality although high full width at half maximum for the deep QD sample suggests bimodal QD size distribution. At 10 K, the PL intensities of InAs QDs and GaAs are directly correlated to the position of the QDs within the SC. This can be because of the different laser intensities reaching the QDs in different regions. As a result, electron excitation and radiative recombination are less probable in QDs buried deep in the base, hence the lower intensities.

Fig. 2*b* shows the PL spectra at 300 K with GaAs and InAs QDs peak positions red-shifted to 870 and ~1080 nm, respectively. As the temperature rises, the PL intensity of reference QD sample has decreased more dramatically than base QD samples. This indicates that reference QD samples are more susceptible to the carrier escapes at RT [10, 17]. QDs embedded within the intrinsic region experience an internal electric field, and such field can assist carriers to escape via field-assisted tunnelling. On the other hand, QDs located in quasi-neutral regions, i.e. flat energy bands do not undergo this internal field hence less carrier escapes out of the QDs. Another interesting feature shown in the PL spectra is the consistent GaAs emission for samples at both low temperature and RT. When the QDs are located in the intrinsic region, the GaAs emission is the lowest. With QDs moving away from the intrinsic region, the GaAs emission increases, indicating fewer carriers migrating to QDs and recombined.

Fig. 3 presents the EQE spectra of the QDSCs. In linear-scaled EQE spectrum, a sharp decrease of photocurrents at 870 nm is in response to the GaAs bandgap. In the supra-bandgap region (400–900 nm), the reference QD sample shows an increasing current contribution whereas the base QD samples have a declining EQE. The cause of the decline is due to reduced carrier collection. By embedding QDs in the base region, the holes have reduced diffusion length due to the presence of QDs. Photocarriers are lost, i.e. recombined, before contributing to current. As a result, the photocurrent reduces for photons with wavelength around 700–870 nm which mainly absorbed in the base region. Particularly, the shallow QD sample with QD closer to the depletion region has led to a shorter hole diffusion length and higher recombination probability compared to the deep QD sample and thus lower photocurrent. Peaks at 915 nm originates from the Wetting layer (WL), and for the same reason, the reference QD sample shows far greater current contribution around this wavelength.

The inset of Fig. 3 shows the log-scaled EQE spectrum. In the sub-bandgap region (950–1100 nm), all QDSC samples show current contribution in this region. In the same regard, the decreases in EQE for shallow and deep QD samples caused by poor carrier collection can be explained by capturing the photocarriers from the base regions in the QDs and their further recombination. In contrast, when QDs are placed in the drift region, photoexcited carriers in the QDs can be efficiently collected and result in a higher photocurrent.

The *J*–*V* characteristics of the QDSCs are shown in Fig. 4 and Table 1. Reference QD sample has the highest J_{sc} of 13.78 mA/cm^2, and however, due to a low V_{oc}, the η is the lowest at 7.52%. This *J*–*V* pattern is anticipated from the EQE spectra (Fig. 3), the high current contribution between supra-bandgap and sub-bandgap would result in a high J_{sc}. However, the continuous states within the WL can reduces the effective bandgap between IB and CB, resulting in a decreased V_{oc} [17]. Additionally, according to the PL study, the higher radiative recombination in GaAs regions may also increase the V_{oc}, when the QDs placed in the base region. The

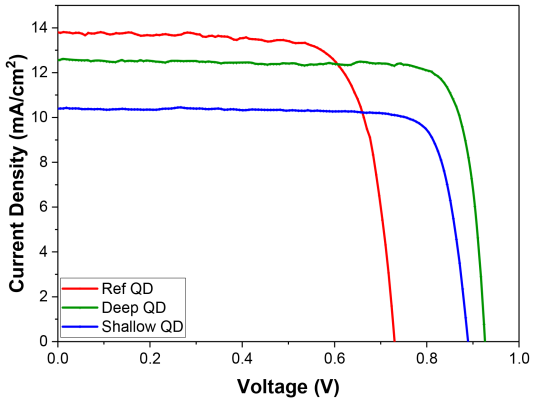

Fig. 4 *Current density versus voltage characteristics for QDSCs under 1 sun (AM1.5G) illumination*

Table 1 J-V Characteristics

Device	J_{sc}, mA/cm^2	V_{oc}, mV	*FF*, %	η, %
ref QD	13.78	730.02	74.67	7.52
deep QD	12.58	926.20	83.63	9.75
shallow QD	10.40	889.53	82.46	7.63

inclusion of QDs within the intrinsic region may introduce defect states and hence act as recombination centres which would further decrease the V_{oc}.

The shallow and deep QD samples have achieved V_{oc} of 889 and 926 mV, respectively. By removing QDs from the intrinsic region, the GaAs material quality is preserved. In terms of J_{sc}, the shallow and deep QD samples have less J_{sc} compared to the reference QD sample. The reduction in J_{sc} is attributed to the poor carrier collection. Deep QD sample with a longer carrier diffusion length has achieved a higher J_{sc}. Despite less carrier collection, the η of shallow and deep QD samples are higher than the ref QD sample. In particular, the deep QD sample has obtained a η of 9.75% which is 29% greater with regard to the ref QD sample. However, the photocurrent generated from QDs are significantly reduced when QDs are deeply buried in the base. In order to increase the contribution of QDs to photocurrent, more QDs or new structure need be implemented.

4 Conclusion

In summary, we present results of QDs in different base regions and compare with a reference QDSC. Both samples with QDs embedded in the base regions have shown higher V_{oc} (27%) with respect to the reference QDSC's. This is due to suppressed carrier recombination via QDs, along with maintaining the effective bandgap. Despite of the benefits offered by the design, there is one drawback, lower carrier collection, which leads to a J_{sc} reduction by more than 1.2 mA/cm^2. This amount of decrease is not insignificant compared to the enhancement made in power conversion efficiency, and this factor should be taken into account with caution in future investigations. Although the photocurrent generation via QDs is yet to be improved, the findings presented here provide an easy means to overcome the voltage loss in QDSC.

5 References

[1] Shockley, W., Queisser, H.J.: 'Detailed balance limit of efficiency of p–n junction solar cells', *J. Appl. Phys.*, 1961, **32**, (3), pp. 510–519

[2] Guter, W., Schöne, J., Philipps, S.P.: 'Current-matched triple-junction solar cell reaching 41.1% conversion efficiency under concentrated sunlight', *Appl. Phys. Lett.*, 2009, **94**, (22), p. 223504

[3] Ross, R.T., Nozik, A.J.: 'Efficiency of hot-carrier solar energy converters', *J. Appl. Phys.*, 1982, **53**, (5), pp. 3813–3818

[4] Luque, A., Martí, A.: 'Increasing the efficiency of ideal solar cells by photon induced transitions at intermediate levels', *Phys. Rev. Lett.*, 1997, **78**, (26), pp. 5014–5017

[5] Luque, A., Martí, A., Stanley, C.: 'Understanding intermediate-band solar cells', *Nat. Photonics*, 2012, **6**, (3), pp. 146–152

[6] Martí, A., Antolín, E., Stanley, C.R.: 'Production of photocurrent due to intermediate-to-conduction-band transitions: a demonstration of a key operating principle of the intermediate-band solar cell', *Phys. Rev. Lett.*, 2006, **97**, (24), p. 247701

[7] Okada, Y., Morioka, T., Yoshida, K.: 'Increase in photocurrent by optical transitions via intermediate quantum states in direct-doped InAs/GaNAs strain-compensated quantum dot solar cell', *J. Appl. Phys.*, 2011, **109**, (2), p. 024301

[8] Oshima, R., Takata, A., Okada, Y.: 'Strain-compensated InAs/GaNAs quantum dots for use in high-efficiency solar cells', *Appl. Phys. Lett.*, 2008, **93**, (8), p. 083111

[9] Hubbard, S.M.: 'Nanostructured photovoltaics for space power', *J. Nanophotonics*, 2009, **3**, (1), p. 031880

[10] Lam, P., Hatch, S., Wu, J.: 'Voltage recovery in charged InAs/GaAs quantum dot solar cells', *Nano Energy*, 2014, **6**, pp. 159–166

[11] Kim, D., Tang, M., Wu, J.: 'Si-doped InAs/GaAs quantum-dot solar cell with AlAs cap layers', *IEEE J. Photovolt.*, 2016, **6**, (4), pp. 906–911

[12] Sablon, K.A., Little, J.W., Mitin, V.: 'Strong enhancement of solar cell efficiency due to quantum dots with built-in charge', *Nano Lett..*, 2011, **11**, (6), pp. 2311–2317

[13] Driscoll, K., Bennett, M.F., Polly, S.J.: 'Effect of quantum dot position and background doping on the performance of quantum dot enhanced GaAs solar cells', *Appl. Phys. Lett.*, 2014, **104**, p. 023119

[14] Walker, A.W., Thériault, O., Wilkins, M.M.: 'Positioning and doping effects on quantum dot multi-junction solar cell performance', *Prog. Photovolt.*, 2014, **23**, (6), pp. 793–799

[15] Liu, H., Sellers, I.R., Gutiérrez, M.: 'Influences of the spacer layer growth temperature on multilayer InAs/GaAs quantum dot structures', *J. Appl. Phys.*, 2004, **96**, (4), pp. 1988–1992

[16] Tutu, F.K., Sellers, I.R., Peinado, M.G.: 'Improved performance of multilayer InAs/GaAs quantum-dot solar cells using a high-growth-temperature GaAs spacer layer', *J. Appl. Phys.*, 2012, **111**, (4), p. 046101

[17] Tutu, F.K., Lam, P., Wu, J.: 'Inas/GaAs quantum dot solar cell with an AlAs cap layer', *Appl. Phys. Lett.*, 2013, **102**, (16), p. 163907